Available online at www.sciencedirect.com
SCIENCE DIRECT
Polymer 46 (2005) 6050–6063
polymer
www.elsevier.com/locate/polymer

Evolution of lamellar orientation and crystalline texture of various polyethylenes and ethylene-based copolymers in plane-strain compression

Z. Bartczak*, E. Lezak

Centre of Molecular Macromolecular Studies, Polish Academy of Sciences, Sienkiewicza 112, 90-363 Lodz, Poland

Received 25 January 2005; received in revised form 19 April 2005; accepted 21 April 2005
Available online 14 June 2005

Abstract

Deformation-induced orientation behavior of a series of polyethylenes and ethylene copolymers was studied by WAXS and SAXS. Plane-strain compression was employed as a deformation mode. Compression experiments were performed at room temperature and at 80 °C. Activity of crystallographic slip systems supported by interlamellar shear during deformation process resulted in formation of the (100)[001] primary texture component with chain axis aligned along the flow direction, FD, and (100) planes perpendicular to the loading direction, LD. A second texture component was produced on unloading by {310} twinning of primary component. Intensity of that twinning was controlled primarily by the molecular weight of polymer, through modification of the molecular network and its stress response on applied strain. Molecular weight influenced also the orientation behavior on the lamellar level. In all polymers studied the lamellar shear, intensive on the beginning of deformation and exhausting around the true strain of 0.75, induced cooperative kinks of lamellae. In samples of relative low molecular weight further advancement of deformation led to an additional intense fragmentation of lamellar structure and restructurization into new long period in the direction of flow ($e > 1.2$). In polymers of higher molecular weight such an intense fragmentation did not occur due to topological constraints. Consequently, the lamellar structure of heavily deformed polyethylenes of low molecular weight consisted of relatively small blocks, oriented with their normals approximately along FD, while high molecular weight species, in absence of intense lamellae fragmentation, developed the structure of relatively long lamellar crystals, oriented in a chevron-like structure. It was found that the orientation produced by deformation process is controlled entirely by the strain applied to the material, while the differences induced by modification of the stress due to the change of the deformation temperature are of minor consequence.

Keywords: Polyethylene; Compression; Texture

1. Introduction

Deformation-induced orientation, greatly improving mechanical properties of semicrystalline polymers, has been widely used for a variety of applications, e.g. drawing of fibers or films. These applications have provided the driving force for a vast number of experimental studies on deformation of semicrystalline polymers, including polyethylene, studied most frequently as a model polymer, under various deformation modes. The mechanisms underlying deformation were reviewed by several authors, e.g. [1–3].

It is now well established that the plastic deformation of semicrystalline polymers involves several mechanisms of deformation of crystalline and amorphous phases. Among them the slip along certain crystallographic planes, twinning, and martensitic transformations are the most widely reported mechanisms of deformation of crystalline component. Interlamellar sliding (shear) and interlamellar separation are the known processes of deformation of amorphous phase [4,5].

Experimental studies of deformation of polyethylene evidenced that the most important deformation mechanisms for crystalline phase are two chain slip processes (100)[001] and (010)[001], supported by the transverse slip of (100)[010] mode [1,2]. The respective critical shear stresses were directly determined for HDPE as 7.2, 15.5 and 12.2 MPa, respectively, at room temperature [6]. The slip systems, especially the easiest (100)[001] chain slip, were found to be active from the very beginning of plastic deformation [7,8]. Simultaneous activity of several slip systems, supported by

* Corresponding author. Tel.: +48 426 803 237; fax: +48 426 847 126.
E-mail address: bartczak@bilbo.cbmm.lodz.pl (Z. Bartczak).

0032-3861/$ - see front matter © 2005 Elsevier Ltd. All rights reserved.
doi:10.1016/j.polymer.2005.04.092

shear deformation of amorphous layers (interlamellar sliding) allows the initial structure to be transformed in a continuous manner into the final oriented state [3].

For the amorphous phase, two modes of plastic deformation have been proposed: interlamellar sliding and lamellar separation [4,5]. According to the study of Galeski et al. [7,8] deformation of amorphous component by interlamellar sliding, being the easiest deformation mechanism to initiate, was prominent only at relatively low strain. While this amorphous sliding began to 'lock' as the molecular extension of tie molecules as well as the segments immobilized by entanglements increased, an enhancing activity of crystallographic slips was observed. The understanding of preferred process of lamellar sliding is properly descriptive, yet it does not provide any information about chain rearrangement within the amorphous region. Since the nature of the amorphous material in thin layers between lamellae is not well known, the mechanism of plastic deformation in the amorphous phase remains still not well understood.

It is known that thermal history and molecular characteristics of a polymer exert marked influence on the mechanical properties of polyethylene [9–12]. Studies of the macroscopic behavior demonstrated that the yield stress increases with percentage of crystallinity and the thickness of the crystallites [13–20]. The higher yield stress in materials of higher crystallinity results from the increased amount of crystalline component which can support higher stresses than the amorphous component. Increasing thickness of lamellae results in deceleration of thermal nucleation of dislocations necessary to activate crystallographic slip processes, which in turn, leads to an increase of the observed yield stress [15]. Moreover, for samples exhibiting similar amount and dimensions of crystallites, the yield stress was reported to increase with increasing molecular weight [9,12], probably due to an increase of network density of the molecular network within amorphous component (network formed by tie molecules and entangled chains), which allows the interlamellar regions as well as lamellae to support higher stresses.

This paper is one of the series reporting the findings of the study of plastic deformation and strain recovery of a series of commercial grade polyethylenes, covering broad range of molecular weight, chain architecture and crystallinity degree. In the other paper [19] we reported the mechanical properties and recovery behavior of these materials. The mechanical deformation tests in plane-strain compression demonstrated the role of the molecular network formed in the amorphous component in the deformation and recovery of semicrystalline polyethylene. The aim of the work reported in this paper was to investigate the evolution of lamellae orientation and crystalline texture accompanying deformation as a function of chain architecture, molecular weight and the state of crystalline component. Similarly to the previous studies the plane-strain compression was chosen as a deformation mode. Plane-strain compression is kinematically similar to tension, yet the deformation proceeds homogeneously (no necking or other discontinuities observed in tension) and can be interrupted at any strain to probe the resultant texture. Additional motivation of this choice is absence of voiding. Formation of voids, frequently observed in tension, modifies the deformation behavior and obscures the real deformation mechanisms underneath. In some cases voiding begins even prior to yield point, which in turn changes dramatically the entire deformation process. Voids produced in drawing, give the high intensity scattering of X-ray at small angles (SAXS), frequently overwhelming lamellar scattering, which makes the study of lamellar orientation very difficult. On contrary, in the absence of voids, the lamellar signature in SAXS patterns of compressed samples is usually clear. Despite these advantages, only a few compression studies of polyethylene have been reported [7,8,20,21].

2. Experimental

2.1. Materials and sample preparation

The materials used in this study were samples of various grades of commercial polyethylene, including five linear high-density polyethylenes (HDPE) of various molecular mass, two samples of ultra-high molecular mass polyethylene (UHMWPE), five conventional branched polyethylenes of different branching level and molecular mass (LDPE) and four copolymers of ethylene with various content of butene-1 or octene-1 comonomer (linear low density polyethylenes, LLDPE, and ethylene-octene1 elastomers). One of LLDPE's (LL-1) was synthesized with metalocene catalyst, while the other (LL-2) was produced with conventional Ziegler-Natta catalyst system. Both ethylene elastomers (E-1, E-2) were of metalocene type. All materials studied are summarized in Table 1.

Samples for deformation experiments, in the form of 50×50 mm^2 and 3.85 mm thick rectangular plates, were prepared by compression molding at the temperature of 190 °C (230 °C for UHMWPE specimens) and pressure of 5 MPa. The compression molded sheets were solidified by fast cooling (quenching) in an iced water. Specimens of the desired size for deformation studies were machined out from these plates. All samples were crystallized under identical thermal conditions in order to obtain specimens of similar initial supermolecular structures [19].

2.2. Plane-strain compression

Plane-strain compression was chosen as the deformation mode throughout this study. The plane-strain compression tests were performed using loading frame of 50 kN capacity (Instron, Model 1114) and a compression tool of the type of deep channel-die [22], equipped with a load and strain gauges as well as heaters connected to the temperature

Table 1
The characteristics of polymers studied

Sample code	Manufacturer	M_w	M_w/M_n	Number of branches (1/1000C)	Density (g/cm^3)	Crystallinity (wt.%)[a]	Long period (nm)[b]	Crystalline stem length (nm)[c]
a. Linear polyethylenes (HDPE, UHMWPE)								
H-1	Quantum	0.57×10^5	3.5	<0.1	0.957	72.7	23.5	20
H-2	BASF	0.76×10^5	4.4	<0.1	0.957	73.3	23.3	19.5
H-3	BASF	1.2×10^5	3.4	<5	0.942	62.6	22.2	16.4
H-4	BASF	1.83×10^5	7.2	<0.2	0.956	67.7	24.4	20.7
H-5	BASF	4.78×10^5	12.2	<3	0.953	60.9	26.0	21.2
U-1	Ticona	$\sim2\times10^6$			0.928	48.9	33.3	18.2
U-2	Ticona	$\sim5.5\times10^6$			0.928	49.6	33.3	17.4
b. Branched polyethylenes (LDPE)								
L-1	BASF	2.5×10^5		20	0.922	46.3	13.2	8.1
L-2	BASF	3.3×10^5		24	0.922	44.4	12.8	7.6
L-3	BASF	4.5×10^5	13.0	35	0.919	40.4	12.3	6.9
L-4	BASF	2.0×10^5	4.0	35	0.919	40.0	11.6	7.1
L-5	BASF	0.48×10^5	3.7	35	0.917	40.0	11.0	6.6

Sample code	Manufacturer	M_w	M_w/M_n	Comonomer type	Comonomer content (mole %)	Density (g/cm^3)	Crystallinity (wt.%)[a]	Long period (nm)[b]	Crystalline stem length (nm)[c]
c. Ethylene copolymers (LLDPE, Ethylene-octene rubbers)									
LL-1	Elenac	0.71×10^5	2.4	butene-1	4.0	0.918	43.0	13.9	8.3
LL-2	Elenac	0.92×10^5	4.0	butene-1	4.1	0.918	41.6	16.1	10.7
E-1	Exxon	0.82×10^5	3.7	octene-1	8.2	0.902	30.1	11.5	5.4
E-2	Dow-DuPont Elastomers	3.67×10^5	2.1	octene-1	14.4	0.870	10.9	11.0	2.0

[a] Estimated on the basis of the heat of melting (DSC).
[b] Estimated from SAXS.
[c] Estimated on the basis of temperature of the melting peak (DSC).

controller. The channel-die is shown schematically in Fig. 1. The channel was 3.85 mm wide, 50 mm long and 60 mm deep, so that samples up to 40 mm high (i.e. along loading direction) could be compressed with that die.

An advantage of a deep channel-die is that the samples

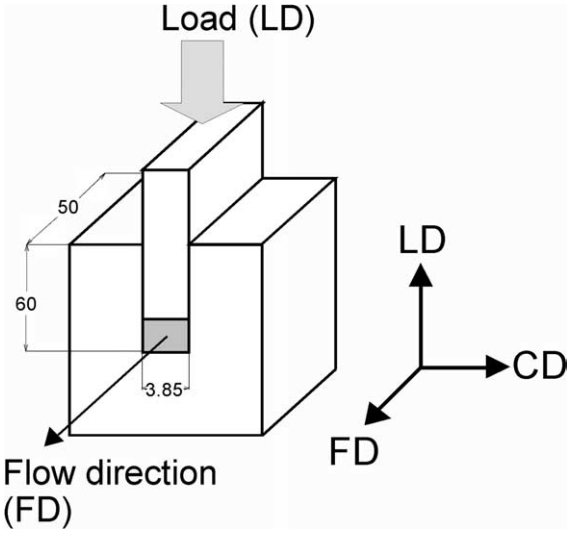

Fig. 1. Schematic view of a channel-die used for deformation experiments. The compressed sample is marked with gray. LD, FD and CD denote the directions of loading, material flow and constraints, respectively.

produced by compression in such a die are relatively large, sufficient for other experiments. The initial size of the specimens used in channel-die compression was $3.85\times50\times40$ mm^3 (width, length and height respectively). After compression to the deformation ratio of 10 the dimensions of the specimen were $3.85\times50\times4$ mm^3, so that the structure and orientation produced by plastic deformation in such large specimens could be studied relatively easy.

All deformation experiments were performed with a constant speed of the crosshead of the loading frame. That speed was set to give the initial deformation rate of 5% per min (8.3×10^{-4} s^{-1}). Deformation tests were performed at room temperature and at the temperature of 80 °C. Specimens and the die were lubricated to reduce the friction forces.

3. Characterization

3.1. DSC

The thermal analysis of the samples was conducted using a TA 2920 DSC apparatus (TA Instruments), indium calibrated. The 5–8 mg specimens were cut out from the core of the compression molded sheets. The melting thermograms were recorded at the heating rate of

10 °/min, under nitrogen flow. The crystallinity level and length of crystalline stem, l^*, were estimated on the basis of heat of melting of the sample recorded during heating from −20 to 180 °C and from the recorded melting temperature, T_m, respectively. For the determination of l^* the Gibbs-Thompson equation was used [23]:

$$l^* = \frac{2\sigma_e T_m^0}{\Delta h_f (T_m^0 - T_m)} \quad (1)$$

where σ_e is the lamellar basal surface free energy (for PE $\sigma_e = 9 \times 10^{-6}$ J/cm^2 [24]), Δh_f is the heat of fusion per unit volume ($\Delta h_f = 293$ J/cm^3 [25]), T_m^0 is the extrapolated equilibrium melting temperature (145.5 °C as estimated for infinitely thick crystals in PE of infinite molecular mass [26]).

3.2. SAXS

Lamellar structure of raw as well as deformed samples was probed by 2-dimensional small angle X-ray scattering (2-D SAXS). The 1.1 m long Kiessig-type camera was equipped with a tapered capillary collimator (XOS) combined with additional pinholes (300 μm in diameter) forming the beam, and an imaging plate as a detector and recording medium (Fuji). The camera was coupled to a X-ray source (sealed-tube, fine point Cu K_α filtered radiation, operating at 50 kV and 40 mA; Philips). The time of collection of the pattern was usually around 3 h. Exposed imaging plates were read with Phosphor Imager SI scanner and ImageQuant software (Molecular Dynamics). In order to obtain the pattern in a particular plane, the slice approx. 2 mm thick, was cut out from the deformed sample in the plane of interest and then examined with SAXS. Long periods were determined from one dimensional sections of 2-D pattern. Background and Lorentz corrections were applied to the curves. Long period was then calculated from position of the maximum of corrected curves using the Bragg law.

3.3. WAXS

The texture of deformed samples was studied using the X-ray pole figure technique (for overview of this technique see e.g. Ref. [27]). A WAXS system consisted of a computer controlled pole figure attachment associated with a wide angle goniometer coupled to a sealed-tube source of filtered Cu K_α radiation, operating at 30 kV and 30 mA (Philips). The specimens in the form of slices approximately 2 mm thick were cut out from the deformed samples in the plane perpendicular to flow direction (FD). Such an orientation of specimens allowed to reduce an influence of analytical errors resulting from defocusing of the beam when the specimen was tilted during data collection. The other details of the technique of pole figure preparation was described elsewhere [6]. The following diffraction reflections from orthorhombic crystal form of PE were analyzed: (110), (200), (020) and (002), positioned at $2\Theta = 21.6$, 24, 36.4 and 74.4°, respectively.

4. Results and discussion

Table 1 presents the characteristics of the samples used for deformation. Their weight crystallinities were determined from DSC data. The length of crystalline stem was estimated from the temperature of the melting peak using Eq. (1). Long period values for unoriented samples were calculated from Lorentz corrected SAXS curves. These data show, that there are large differences in crystalline structure parameters among the groups of polymers which differ in chain architecture (i.e. linear PE, branched, PE, copolymers) while the differences within any group are much smaller, e.g. the group of linear samples shows the crystallinity within the range of 60–70 wt%, while samples of branched PE's have the crystallinity between 40 and 46 wt%. The largest differences in crystallinity varying from 10 to 43 wt% can be found among copolymers due to large variation in comonomer content in these polymers. On the other hand, the supermolecular structure of the samples was similar: in nearly all samples a spherulitic structure was observed, with an average radius varying from a few to more than 10 μm [19]. The only exceptions were the samples of U-1 and U-2 (UHMWPE) and E-2 (ethylene-octene-1 elastomer), in which lamellae were oriented randomly and not organized in spherulites.

In the first deformation experiment the samples of polymers studied were deformed by plane-strain compression at room temperature to the compressive true strain around $e = 2$ (the respective compression ratio above CR = 7; the compressive true strain was determined from the following equation:

$$e = \int_{h=h_0}^{h=0} \frac{dh}{h} = \ln\left(\frac{h_0}{h}\right) = \ln\left(\frac{h_0}{h_0 - \Delta h}\right) = \ln(\mathrm{CR}) \quad (2)$$

where h_0 denotes the initial height of the specimen, $h = h_0 - \Delta h$ represents its actual height, Δh is the measured displacement of the plunger and $\mathrm{CR} = h_0/h$ is the compression ratio). The stresses generated in compression to such high strains frequently exceeded the level of 500 MPa [19]. Due to the strain recovery after unloading the samples retained only a part of the strain imposed during the deformation in a channel-die. The applied strains and their recovered and permanent parts are reported in Table 2. The recovery behavior of these materials was discussed in a separate paper [19].

Figs. 2 and 3 present the 2-dimensional patterns of the deformed specimens of linear polyethylenes studied (HDPE, UHMWPE). The SAXS patterns of deformed specimens were collected after their complete recovery (at least 1 month at room temperature). For every deformed

Table 2
Parameters determined from 2-D SAXS patterns of samples deformed at room temperature

Sample	LP (unoriented) (nm)	Strain applied, $e_{applied}$	Recovered strain, $e_{recov.}$	Permanent strain, $e_{recovered}$	LP-CD view pattern			LP–LD view
					Along FD (nm)	At max. (nm)	Angle to FD (°)	along FD (nm)
H-1	23.5	2.01	0.19	1.82	15.4	10.9	45	14.7
H-2	23.3	2.03	0.18	1.85	14.5	11.4	38	14.1
H-3	22.2	1.98	0.21	1.77	14.7	10.2	46	14.7
H-4	24.4	1.99	0.24	1.75	15.9	11.1	46	16.1
H-5	26.0	1.91	0.30	1.61	16.1	10.4	50	16.1
U-1	33.3	1.60	0.52	1.08	21.7	11.8	52	20.8
U-2	33.3	1.62	0.58	1.04	21.7	13.1	54	22.0
L-1	13.2	2.01	0.32	1.69	9.7	7.2	42	9.2
L-2	12.8	1.76	0.32	1.44	9.6	7.1	43	9.3
L-3	12.3	2.01	0.36	1.65	9.8	7.0	44	9.8
L-4	11.6	1.95	0.33	1.62	9.8	7.4	41	9.8
L-5	11.0	1.96	0.33	1.60	9.6	7.5	38	9.5
LL-1	13.9	1.86	0.55	1.31	11.1	7.4	48	11.0
LL-2	16.1	2.01	0.44	1.57	11.2	7.2	50	11.3
E-1	11.5	2.08	0.81	1.27	10.4	7.0	47	10.3
E-2	11.0	2.03	1.51	0.52	11.4	9.5	35	11.4

sample two patterns are presented: one obtained in the LD–FD plane (X-ray illumination along constraint direction, CD; see Fig. 1 for explanation of coordinates), and the other in the FD–CD plane (X-ray beam parallel to loading direction, LD). The FD–LD patterns obtained for deformed linear polyethylenes (cf. Fig. 2) show the systematic variation of their shape, which seems to correlate with an increasing molecular weight. In sample H-1 of low molecular weight ($M_w = 0.57 \times 10^5$) the 2-D pattern has a shape of two lines perpendicular to FD and slightly curved outwards. Scans along these lines revealed a single low and broad maximum, centered around FD. Similar pattern consisting of two lines was observed in sample H-2 ($M_w = 0.76 \times 10^5$), although two low maxima developed along each line near its ends can be recognized instead of single one centered along FD, as observed for H-1. Additionally, both H-1 and H-2 patterns (FD–LD) show short equatorial streaks, presumably related to voids oriented parallel to FD. Most probably, these voids formed on unloading, since the compression stress component during deformation process should inhibit any void formation. The patterns obtained for samples H-3, H-4 and H-5 of increasing molecular weight (M_w above 10^5) continuously evolve from linear towards 4-point pattern. Although a trace of lines can be still observed here, the four maxima along lines develop higher and become dominate the pattern with increasing molecular weight, while the saddles between maxima, near FD, deepen substantially. This tendency continues in samples of UHMWPE, in which clear 4-point patterns can be observed in the FD–LD plane (cf. Fig. 3). Another feature of the FD–LD patterns of samples of M_w above 10^5 (H-3–U-2) is that the void scattering is no longer present here.

Figs. 2 and 3 present also the patterns collected in the FD–CD plane (the right-hand side row). It can be seen that for all linear materials these patterns are similar, 2-point patterns, with two maxima oriented along FD.

Table 2 reports long periods estimated along several directions of interest from the discussed above patterns and the characteristic angles between the direction of maximum in 4-point pattern and the direction of flow, FD. These data show good agreement of long period along FD determined from both FD–LD and FD–CD patterns. For all deformed samples of linear PE's the value of that long period is much smaller than the long period of the respective sample prior to orientation. Moreover, the long period determined along the direction of the maximum is even smaller, less than a half of the initial value. The direction of maximum stays around 50° away from FD in all patterns of this series (see Table 2). The maxima stay roughly 40–50° away from FD in all patterns of this series (see Table 2).

The shape of the reported patterns suggests that in linear polymers lamellae orienting with their normals in the FD–LD plane during the deformation process undergo substantial thinning and presumably some fragmentation. Large reduction of the long period measured along FD and even larger, when estimated along azimuth defined by developed maxima, indicate an intense plastic deformation of these lamellae by chain slip processes [1–3,7]. Substantial thinning of lamellae together with the rotation of the chain axis away of lamella normal, both due to intense chain slip, probably led at the advanced stage of deformation to some local instabilities of the slip processes and consequently to fragmentation of lamellae into smaller blocks [7]. That fragmentation seems more severe in the case of lower molecular weight samples as demonstrated by the FD–LD patterns of samples H-1 and H-2, characteristic for the structure consisting of relatively small blocks with their

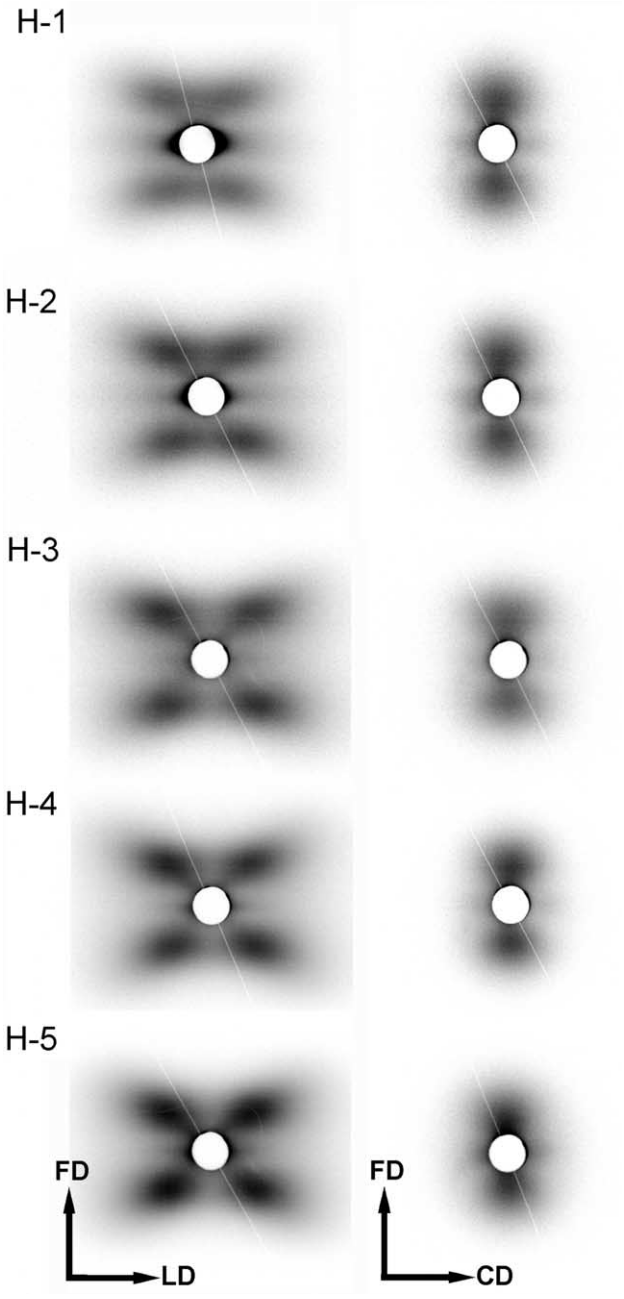

Fig. 2. Two-dimensional SAXS pattern determined for linear polyethylene homopolymers H-1–H-5, deformed to the true strain around 2, at room temperature: left-hand side column-CD view, right hand-side column-LD view.

normals oriented more or less around FD and arranged in a chevron-like array [7,28]. The patterns observed in samples of higher molecular weight suggest that intense crystallographic slip was accompanied by much less fragmentation of lamellae, most probably limited to cooperative kinks (i.e. lamellae broke only locally, but in cooperative fashion, together with their neighbours) [8,29], which produced structure consisting of relatively long lamellar fragments with normals oriented approximately 50° away from FD in the FD–LD plane, arranged in a chevron-like pattern, when

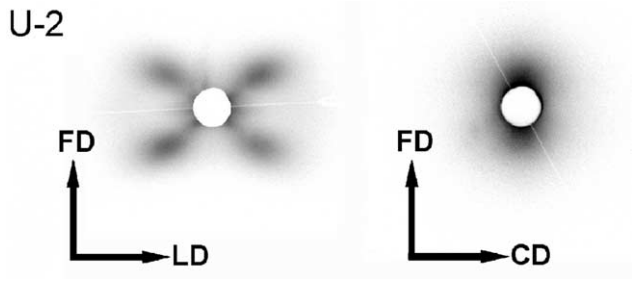

Fig. 3. Two-dimensional SAXS patterns determined for ultrahigh molecular weight polyethylene U-2, deformed to the true strain around 1.6, at room temperature.

observed from CD direction. The suppressed fragmentation of lamellae in samples of high molecular weight results most probably from more constrained structure comparing to low molecular weight counterpart (more tie-molecules, each connecting several crystals, more trapped entanglements in amorphous layers between crystallites and reduced number of loose chain ends). Such a constrained structure with high connectivity among lamellae due to numerous tie molecules is less capable to fragmentation and subsequent reorganization than the structure of low molecular weight samples (relatively little constraints and connectivity at interfaces): higher number of junctions at the crystal-amorphous interfaces and denser molecular network result in more uniform stress distribution along crystal-amorphous interfaces, hence there is less stress concentrations which could lead to slip localization and consequent fragmentation of lamellae.

On the other hand, these lamellae which are oriented with their normals along FD, when probed in the FD–CD plane produce clear 2-point pattern, which indicates relatively large dimensions of the crystallites along CD, i.e. no fragmentation occurred to lamellae in the FD–CD plane, due to external constraints limiting chain slip process in this plane [7,28].

The kinking of lamellar stacks leading to formation of a chevron-like structure is observed also in other deformation modes, e.g. uniaxial compression [8]. It occurs when the lamellae in stack are oriented initially with their normals perpendicular to the direction of compression. In the case of plane-strain compression the main compressive stress acts along LD, while the constraints imposed by the side walls of the channel induce another compressive stress along CD. This stress is approximately a half of that along LD. The presence of two compressive stresses prevents kinking of all lamellae except those oriented initially with their normals along FD. Since the compressive stress along LD is considerably higher than that along CD, kinking occurs preferentially in the LD–FD plane. Consequently, it is observed in the CD-view, while practically absent in the LD-view.

Fig. 4 presents 2-D SAXS patterns of L-4 LDPE, illustrating typical features observed also in other samples

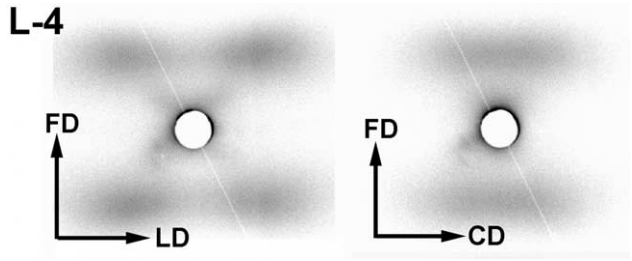

Fig. 4. Two-dimensional SAXS patterns determined for branched polyethylene L-4, deformed to the true strain around 2, at room temperature.

of branched PE's. The FD–LD patterns of all five polymers in this series have quite similar shape, slightly different than the patterns observed for linear samples, probably due to noticeably lower crystallinity level as well as smaller lamellar thickness as compared to linear polymers. The same is true for respective FD–CD patterns. No signature of void scattering could be found in any branched sample. The patterns recorded in the CD view (FD–LD plane) consist of two lines perpendicular to FD. Along each line two clear maxima can be recognized near their ends, separated by the saddle centered in direction of flow. This saddle is deeper in samples of higher molecular weight than in low molecular sample L-5. Because of the presence of clear maxima these patterns can be classified into 4-point type rather than to line pattern. As reported in Table 2 the long period measured along FD or the azimuth defined by maxima is much smaller than in initial unoriented material, which demonstrates intense deformation by crystallographic slips, although advanced less than in linear PE's. The four-point feature indicates the chevron-like arrangement of lamellae, produced presumably by cooperative kinking. An azimuth defined by the intensity maxima is about 40° away from FD, i.e. ca. 10° less than observed for linear PE samples. This may indicate a large contribution of the interlamellar sliding, much reversible on unloading [8,19], which would result in a rotation of the lamella normals away of FD on loading simultaneously with rotation produced by chain slip within crystals, while back-rotation towards FD on unloading. All polymers studied in this paper, when deformed at room temperature demonstrated substantial strain recovery. However, that recovered strain was higher in samples of LDPE's as well as copolymers, all demonstrating relative low crystallinity, as compared to samples of highly crystalline linear PE's. This is illustrated by the strain recovery data presented in Table 2. The recovery behavior of the studied materials was studied in detail in Ref. [19].

The respective LD-view patterns (FD–CD plane) consist of two straight lines, shorter than in FD–LD projection, with a broad maximum centered in FD direction on every line. In the deformed L-5 sample of $M_w = 0.48 \times 10^5$ two arcs are observed rather than lines in the FD–CD pattern. This can indicate more deformation and fragmentation of lamellae oriented with their normals around FD than in deformation of linear PE, in spite of similar strong external constraints imposed. However, the restrictions due to these constraints are now smaller than in highly crystalline linear PE's due to larger amount of amorphous component, which modifies local stress fields for crystals.

Fig. 5 presents exemplary 2-D SAXS patterns collected for samples of ethylene-based copolymers. It can be seen that the patterns obtained for copolymers of relatively low comonomer content and moderate crystallinity as LL-1, LL-2 (not presented) and E-1, exhibit the similar features to these observed in deformed samples of branched PE. However, the patterns obtained for E-2 copolymer are different. The CD-view pattern of this sample consist of elliptical contour in which four clear maxima can be discerned, each located 35° away from FD. The LD-view pattern of the same specimen consist of two arcs in FD direction. These SAXS patterns of E-2 evidence the relative broad distribution of orientation of lamellae with stronger component of preferred orientation characterized by lamella normals oriented in the FD–LD plane approximately 35° away from FD. The data shown in Table 2 demonstrate that there is little reduction of the long period due to deformation, which implies low activity of crystallographic slips within lamellar crystals of E-2 sample. To understand

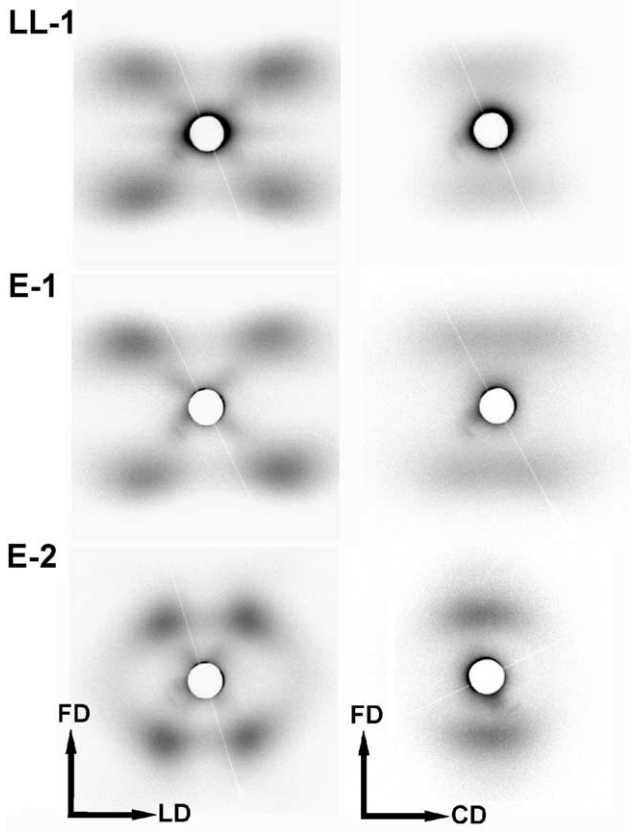

Fig. 5. Two-dimensional SAXS pattern determined for ethylene-based copolymers, LL-1, E-1 and E-2, deformed to the true strain around 2, at room temperature.

these features, we must recall exceptionally low crystallinity of the discussed copolymer, below 10% by volume. For that low crystallinity the lamellae do not form continuous spherulitic structure any longer, opposite to other samples of higher crystallinity. Instead, single isolated lamellae and/or stacks of few lamellae are embedded in a continuous amorphous matrix. Such a morphology promotes deformation mostly by shear of the amorphous phase, highly reversible on unloading, supplemented with relative small contribution from deformation of crystalline component. This view is supported by the observed very high component of the strain recovered on unloading [19] (cf. Table 2). Due to the shear deformation in amorphous embedding the lamellae are forced to rotate and tend to orient with their normals along LD during loading. On unloading a large part of the strain is recovered, which results in a back-rotation of the lamella normals towards FD direction. In this way only a part of the orientation produced by the shear of amorphous component together with that produced by limited slip activity remain permanently in the unloaded and relaxed sample.

In order to follow the evolution of the lamellar orientation with increasing strain the specimens of H-2 (linear PE of relatively low molecular weight) and of L-3 (branched PE of high molecular weight) were deformed to various strains up to $e=2$ and their CD-view and LD-view 2-D SAXS patterns were examined. Fig. 6 presents such patterns collected for sample H-2, while Fig. 7 those obtained for sample L-3. As it was already discussed these polymers when deformed to high strain near $e=2$ exhibit somewhat different patterns (cf. Figs. 2 and 4). Comparison of Figs. 6 and 7 demonstrate the differences in evolution of lamellar orientation in these samples with increasing strains.

Fig. 6 shows that both CD-view (FD–LD projection) and LD-view (FD–CD projection) patterns of H-2 evolve from a circle to an ellipse at strain increasing from 0 to less than 0.75, which suggests the deformation by simultaneous crystallographic slips and interlamellar shear (lamellar sliding). Around $e=0.75$ the 4-point signature emerges in the CD-view pattern, while in LD-view an ellipse is replaced by two arcs oriented along CD. That 4-point feature in CD-view pattern strengthens with further advance of applied strain. Previous studies of deformation of HDPE demonstrated that this transformation originates from an exhaustion, or 'lock', of the interlamellar shear due to almost complete extension of the chain segments immobilized by adjacent crystals and by trapped entanglements [7,8]. Because of connectivity between crystalline lamellae and amorphous layers both phases must deform simultaneously and cooperatively. Thus, further accommodation of the strain at such conditions must lead to fast increase of the stress due to network orientation hardening, and moreover, its additional concentration in the vicinity of crystal-amorphous junction points, where tie-molecules cross the interface. This leads soon to local cooperative breaks of neighboring lamellae and formation of lamellar

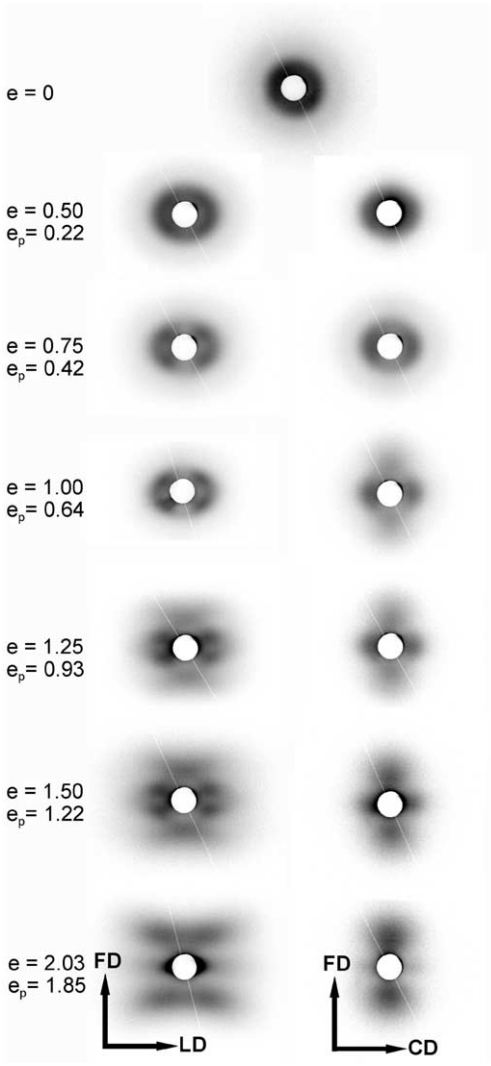

Fig. 6. Evolution of the SAXS patterns as a function of the strain, determined for linear homopolymer H-2, deformed at room temperature. Left hand-side column-CD view, right hand-side column-LD view. Applied strain, e, and permanent strain, e_p, are indicated for each specimen.

kinks, evidenced by TEM observations [8,19]. As a result two lamellar populations develop, each oriented at some acute angle with respect to LD, which produce 4-point scattering. Such limited breaking of lamellae relieves some of constraints in amorphous component and some relaxation of the molecular network, which in turn allows for further interlamellar shear. At the applied strain between 1 and 1.25 the molecular network comes once again near its extensibility limit. At that strain range, however, due to very intense intra-lamellar slips lamellae are already thinned considerably, which eventually precipitates slip instabilities and consequently chain slip localization. As a result an intense fragmentation of lamellae into smaller blocks occurs, followed by unconstrained rotation of these blocks, which results in restructurization into a new long period along FD, emerging below $e=1.25$ [7]. At strain of $e=1.25$ and 1.5 the signatures of both kinked lamellae and a new,

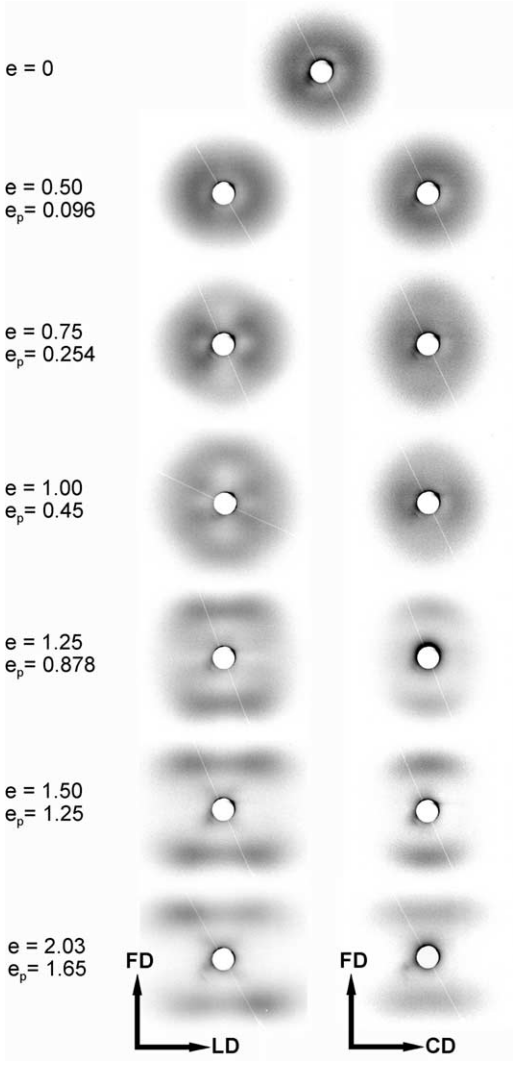

Fig. 7. Evolution of the SAXS patterns as a function of the strain, determined for branched homopolymer L-3, deformed at room temperature. Left hand-side column-CD view, right hand-side column-LD view. Applied strain, e, and permanent strain, e_p, are indicated for each specimen.

fragmented and rotated block structure can be recognized in the CD-view patterns presented in Fig. 6. Finally, at even higher strain, above 1.5, the scattering of the new structure dominates completely the CD-view pattern. The changes in the LD-view patterns at strain above 1.0 follow theses described for CD-view patterns: the new structure with long period along FD gradually replaces the pre-existing one. The outlined above transformation sequence was studied in the past and discussed in details in Ref. [7].

Fig. 7 presents the evolution of lamellar structure of the sample L-3. This polymer has the molecular weight of 4.5×10^5, much higher than H-2 (0.76×10^5) discussed above, and additionally exhibits numerous long branches along the chain. Note, that the four-point feature of the CD-view SAXS pattern observed in L-3 near the final strain of 2 is common for all studied samples of moderate and high molecular weight (cf. Figs. 2–5). Following the evolution of the lamellar structure with increasing strain, demonstrated in Fig. 7, one can find that at low strains, up to $e=1$, the structure of L-3 changes in similar fashion as in already discussed H-2 sample. The transformation of circular pattern of unoriented material, through elliptical, into 4-point occurs in that strain range, due to exhaustion of interlamellar shear prompting cooperative kinks of lamellae, giving rise to formation of 4-point pattern. However, at higher strains only a further reorientation of the structure produced already by kinking can be observed, while there is no signature of heavy lamellar fragmentation nor formation of a new long period. The four-point feature of the CD-view pattern is practically preserved up to the final strain of $e=2$: the SAXS pattern changed gradually with increasing strain and any abrupt transformation of the structure was not detected. In contrast to H-2 discussed above, no signature of a new long period emerges at any strain (compare patterns of H-2 and L-3 deformed to $e\geq1.25$, presented in Figs. 6 and 7, respectively). This demonstrates that the transformation of the lamellar structure through lamellar fragmentation does not occur in materials of high molecular weight. As we already discussed the absence of that transformation is related to that the high molecular weight samples, including branched polymers, have lower crystallinity and thicker interlamellar amorphous layers than the low molecular weight polymers, while the amorphous phase consist of more tie molecules, connecting frequently even several neighboring lamellae, and more chain entanglements, both immobilizing chain segments [19]. This produces highly constrained topological structure with high connectivity among neighboring lamellae. Such a robust structure is much less susceptible to fragmentation than the respective structure of low molecular weight sample, easily undergoing lamellar fragmentation at strain above 1. Consequently, only a limited fragmentation of lamellae, through their cooperative kinking occurs in the deformation of polyethylenes of high molecular weight. This type of behavior was also demonstrated for UHMWPE deformed in plane-strain compression [30].

Figs. 8 and 9 present pole figures determined for the main crystallographic planes of the representative samples, deformed in a channel-die at room temperature. For each sample, except E-2 copolymer discussed later, the pole figures of the (110), (200), (020) and (002) planes of orthorhombic polyethylene were constructed. These pole figures illustrate the preferred orientation of crystalline component produced by plastic deformation. The figures of (200), (020) and (002) show directly the orientation distribution of the **a**, **b** and **c** vectors of the unit cell, respectively, where direction of **c** coincides with direction of chain within crystal. All pole figures presented in this article were normalized, so that intensity of 1.0 is equivalent to the intensity expected for a randomly oriented sample. The scale of the plots was chosen in this way that the white color denotes concentration of poles below that of random

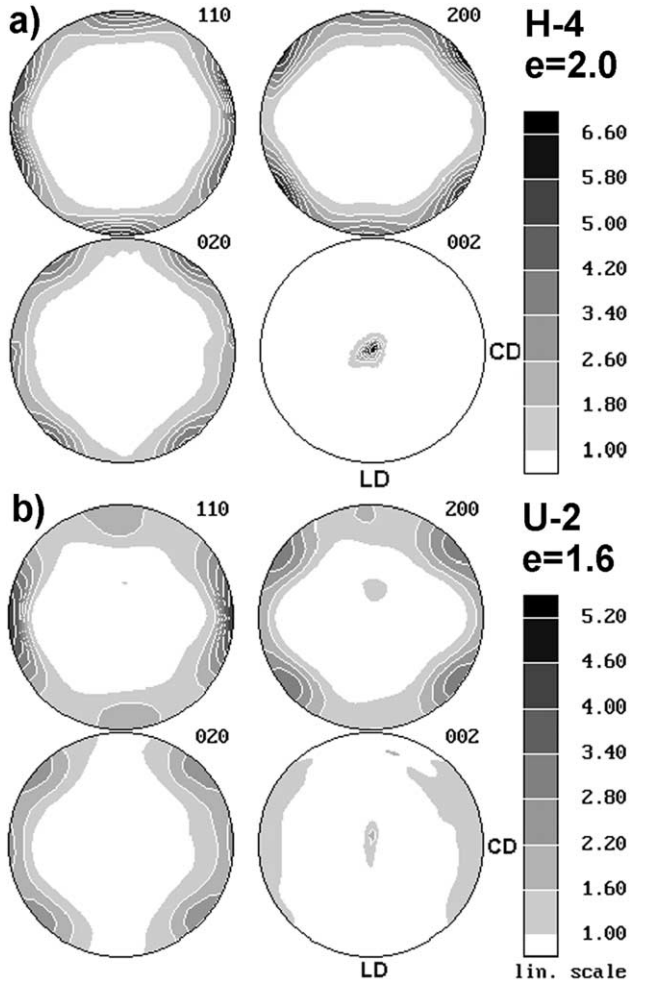

Fig. 8. Representative pole figures of the crystallographic planes (110), (200), (020) and (002) of orthorhombic PE, determined for linear homopolymers H-4 (a) and U-2 (b), deformed at room temperature to the true strain of $e=2$ and 1.6, respectively.

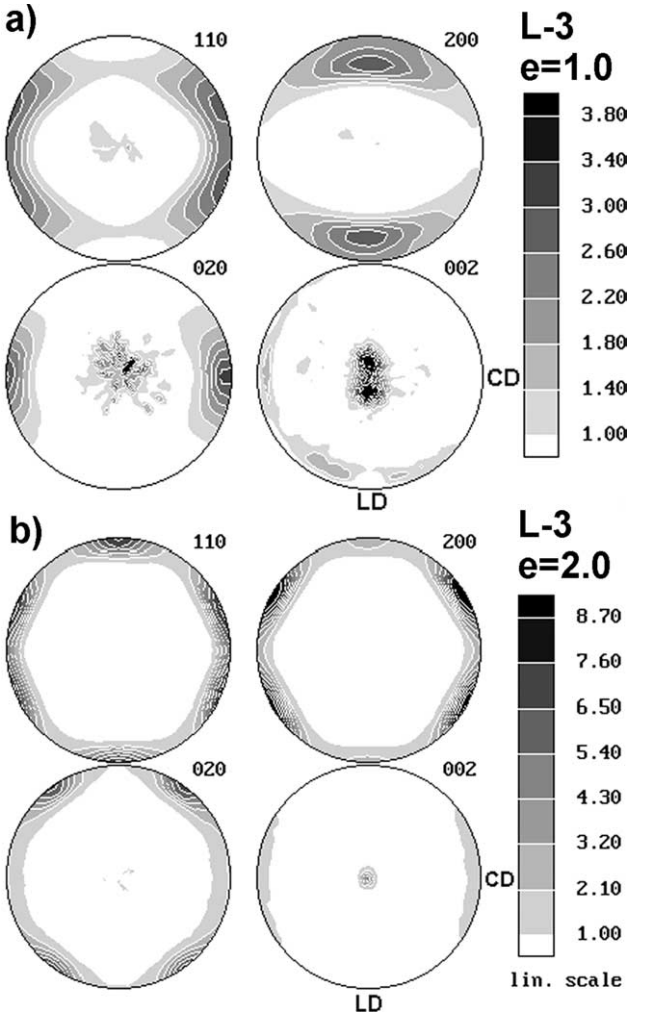

Fig. 9. Pole figures of the crystallographic planes (110), (200), (020) and (002) of orthorhombic PE, determined for branched polyethylene L-3 deformed at room temperature to the true strain of 1.0 (a) and 2.0 (b).

orientation ($I<1.0$), while gray shades and black show the concentrations of poles above average ($I>1.0$).

As can be seen in Fig. 8 the texture of all orthorhombic samples show the same main features. Pole figures of (200), (020) and (110) planes demonstrate poles (i.e. normals to the crystallographic plane of interest) distributed near the equator, i.e. in the LD–CD plane, which evidences that practically all (*hk*0) planes are oriented well with their normals perpendicular to the flow direction, FD. This coincides with the orientation of, **c** axis (direction of chain) expected along FD. This is confirmed by measured pole figures of (002) plane, demonstrating sharp orientation of the (002) poles in direction of FD. In pole figures of (200) plane usually six discernible maxima is distributed along the equator. Two of them are located in loading direction, LD, while other four are tilted $\pm(53-58°)$ away from LD. In (020) pole figures also 6 maxima can be identified in equatorial plane: 2 in direction of CD and 4 located at $\pm(45-56°)$ away from this direction. Pole figures of (110) plane demonstrate again 6 maxima in direction LD (2) and $\pm(70-80°)$ away from LD (4). Such distribution of poles of the discussed planes indicates two-component texture in which both components are oriented with chain direction along FD. First component is that oriented with **a** unit vector along LD, i.e. a component of the (100)[001] type (this conventional notation indicates that [001] direction coincides with machine direction, here FD, while (100) planes are oriented with normals along direction of loading, LD). The second texture component can be identified as the (100)[001] primary component which was rotated around FD axis by approximately $\pm54°$ from LD towards CD. Such an orientation is characteristic for the crystal oriented initially with **a** unit vector along LD which has undergone twinning along {310} plane since the rotation of the unit cell expected for this twinning mode is equal 54° [33,1,2]. Therefore, it can be concluded that the second texture component is the result of {310} twinning of the basic (100)[001] texture component. It was demonstrated [29,33] that such a twinning occurs in the presence of tensile stress along LD direction. For deformation by plane-strain

compression such situation occurs only on unloading, when the tensile stress along LD is generated by recovery forces [29]. If the strain recovery is high in the particulate sample then the tensile stress generated can be high enough to trigger twinning on unloading. This was demonstrated in the series of experiments of plane-strain compression and strain recovery of HDPE at various deformation rates [29]. With increasing strain rate higher stress was induced at both loading and unloading stages. High tensile stress generated on unloading of samples deformed at high rate resulted in intense {310} twinning while the low one, when deformation rate was also low, did not.

The samples of deformed branched polyethylenes and copolymers (except E-2) show the sharp two-component textures of basic and twin components, similar to that observed in HDPE, which is illustrated by pole figures of L-3 sample, presented in Fig. 9(b).

Pole figures of UHMWPE samples U-1 and U-2 (cf. Fig. 8(b)) show practically only the twin component of the texture in contrast to samples of HDPE, LDPE or copolymers, all exhibiting both basic (100)[001] and {310} twin components. It means that in UHMWPE's virtually all crystals of the basic component were transformed on unloading by {310} twinning. This can be understood if one compare the rate of the strain hardening in UHMWPE with that of HDPE's and the respective amount of the strain recovery. In the other paper [19] we have found that both the strain hardening rate and recoverable strain increase substantially with increasing molecular weight and are much larger in UHMWPE than in conventional HDPE. This means that the tensile stress along LD generated on unloading of heavily deformed UHMWPE is much higher than the respective stress in HDPE's deformed to similar strain. This results in nearly complete conversion of the basic orientation component into its twin in samples of ultra-high molecular weight.

The basic component of the texture, i.e. (100)[001] texture was produced in all samples studied during the deformation step. Detailed studies of deformation of HDPE [7,8] revealed that this typo of orientation is a result of an intense and cooperative action of two slip systems-(100)[001] chain slip and (100)[010] transverse slip, supported by interlamellar shear. Other deformation mechanisms appear to play a minor role in production of such a texture and only supplement these two dominant slip systems.

Additional evidence for the (100)[001] as the primary texture component is given in Fig. 9(a). In this figure a set of pole figures determined for sample L-3 deformed to the true strain of $e=1.0$ is presented. Textures found in other samples deformed to comparable strain resemble closely this one, hence are not presented here. At that moderate strain the strain hardening is not advanced yet, and the stress response of the material on the imposed strain is relatively low comparing to the high-strain region. Therefore, the stresses generated on strain recovery are also low, apparently too low to induce noticeable twinning, as confirmed by Fig. 9(a) in which only the primary texture component can be recognized, while there is no trace of any twins. The orientation at $e=1.0$ is less advanced than in the previously discussed samples deformed to true strain around 2 (cf. Fig. 9(b)), thus the texture consist of two identical sub-components, both of the (100)[001] type, yet with [001] axis not aligned precisely along FD, but tilted few degrees from FD towards LD. In reference [7] it was demonstrated that these orientation sub-components rotate gradually toward the final position at FD with increasing strain and finally merge into a single component at strains above 1.2. What important now is the absence of any trace of twinning activity at lower strain. Such a result strongly supports the notion that the twin component is produced on unloading of heavily deformed samples rather than during their compression.

As revealed by preliminary X-ray $\Theta-2\Theta$ scans E-2 copolymer does not crystallize in usual orthorhombic form, as other samples do. Instead, it forms crystals identified as monoclinic modification [31,32]. Therefore, for this sample the pole figures of three planes of (001), (200) and (010) were determined (the diffraction angles 2Θ of 19.6, 23.4 and 36.6°, respectively). We note here that the position of the (010) found in our samples was higher than expected on the basis of unit cell dimensions [31]. Fig. 10 shows the obtained pole figures of E-2 sample deformed to the strain of $e=2.03$. Due to intense strain recovery of this elastomer the permanent strain remaining in the sample was merely $e_p=0.52$. In monoclinic modification the normals of the (010) coincide with the direction of chain in the crystals. It can be observed that poles of the (010) planes cluster primarily around the flow direction and additionally in four regions of the equatorial plane LD–CD. Poles of the (100) plane, giving the strongest diffraction peak, produce two clear maxima in direction of CD, while poles of (200) planes

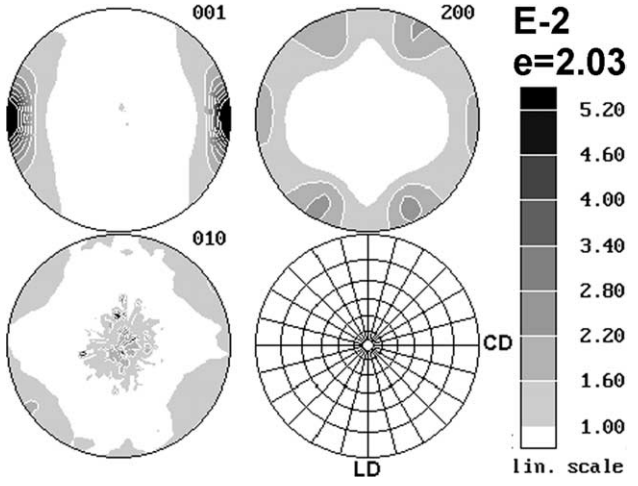

Fig. 10. Pole figures of (001), (200) and (010) crystallographic planes of the monoclinic unit cell measured for E-2 copolymer deformed to the true strain of $e=2.03$, at room temperature. The permanent strain left after unloading was 0.52.

show 6 cluster of higher concentration, all located in the LD–CD plane. This set of pole figures can suggest deformation of crystalline phase by the chain slip systems of the (*h*0*l*)(010) in addition to deformation of amorphous component. However, the experimental evidence is not sufficient to identify exactly the slip plane(s). Unfortunately, there is also no data in the literature concerning the mechanisms of deformation of monoclinic modification of polyethylene since it usually appears in PE materials in rather small quantities, while most of the crystalline component crystallizes in the orthorhombic form. It would be interesting then to study the deformation behavior of this elastomer in more details.

In order to find out the influence of the deformation conditions on the orientation induced by that deformation an another series of deformation experiments was performed at the temperature of 80 °C. Fig. 11 presents selected representative 2-D SAXS patterns of samples deformed at 80 °C to the true strain in the range of 2. Fig. 12 shows the

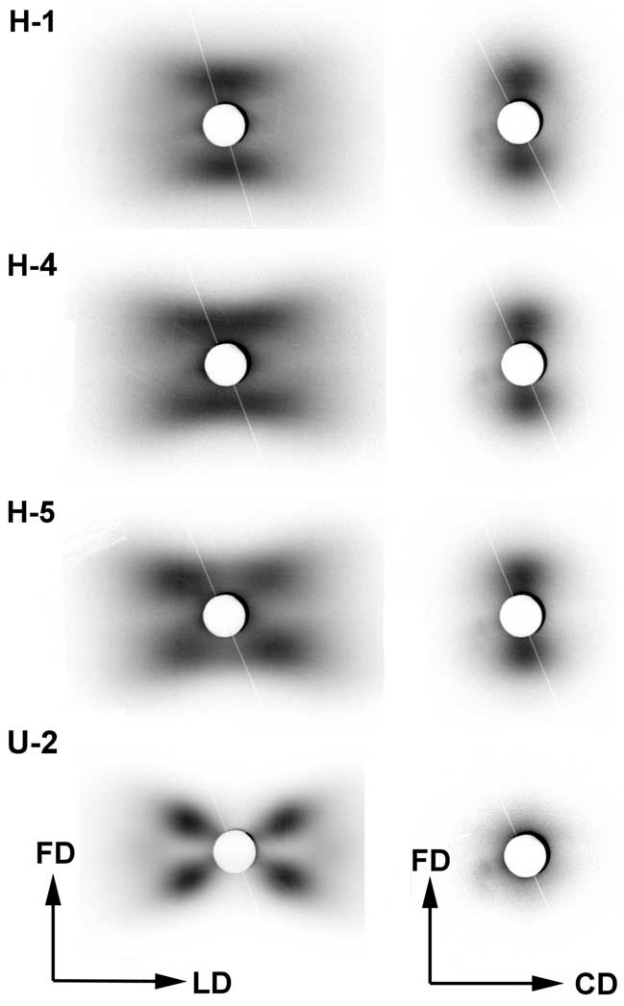

Fig. 11. Two-dimensional SAXS pattern determined for samples H-1, H-4 and H-5 of HDPE and U-2 of UHMWPE, deformed at temperature of 80 °C to the true strain of 2.0, 2.0, 2.0 and 1.68, respectively. Left-side column-CD view, right-side column-LD view.

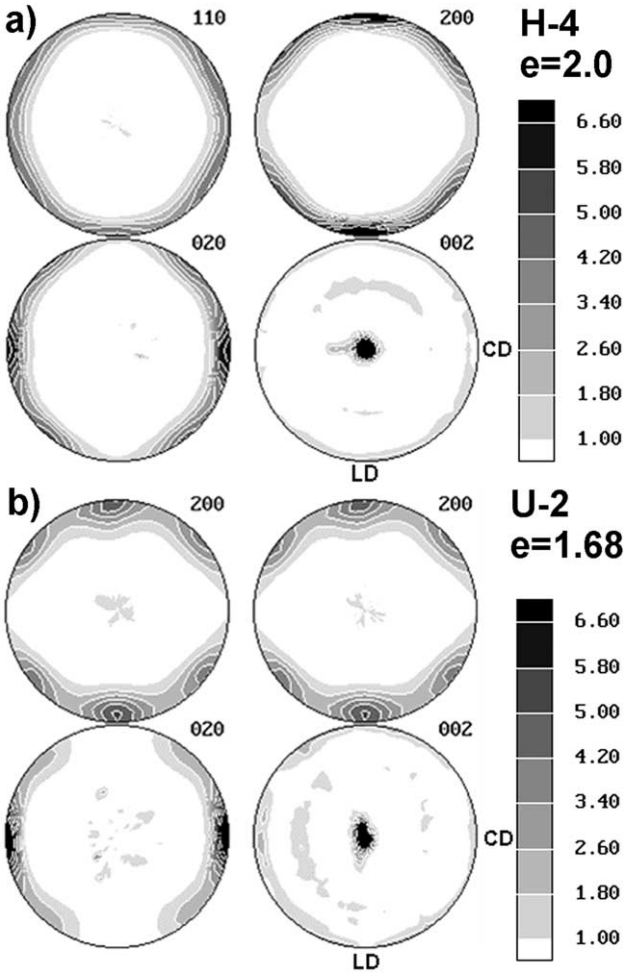

Fig. 12. Pole figures of the crystallographic planes (110), (200), (020) and (002) of orthorhombic PE, determined for samples H-4 (a) and U-2 (b), deformed at temperature of 80 °C to the true strain of $e=2.0$ and 1.68, respectively.

pole figures of the same samples (H-1 and H-5 show textures very close to that of H-4 presented in the figure). It can be found that the SAXS patterns do not differ markedly from the patterns obtained for the same materials deformed at room temperature (cf. Figs. 2–5), which evidence similar orientation of lamellar structure obtained at different temperatures. The same is true for other HDPE, LDPE and copolymer samples (patterns not presented). Also the texture of crystalline component produced by deformation at 80 °C (exemplary pole figures shown in Fig. 12), does not differ substantially from that observed in samples deformed at room temperature. The texture consist again of primary (100)[001] component supplemented by its {310} twin. The only difference between respective samples deformed at elevated and at room temperature is in the fraction of twin component of the texture. In materials deformed at room temperature the fraction of twinned crystals was substantial, or even dominant, as in U-1 and U-2 (UHMWPE). In contrast, in samples deformed at 80 °C the texture is dominated by the primary (100)[001] component, while an

amount of twinned crystals is much lower. In samples of low molecular mass the twin component is barely visible. This behavior can be attributed again to the strain recovery process, during which the tensile stress along LD induces twinning. Samples deformed at elevated temperature develop much lower stresses than those deformed at ambient conditions, which surely influences the intensity of twinning and therefore the final texture of the material. Of course, the dependence on molecular weight is the same as in case of deformation at room temperature-molecular weight, influencing molecular network, controls the strain hardening stage [19] and the stress generated during high-strain deformation and hence the tensile back-stress induced on strain recovery are higher in samples of higher molecular weight. Therefore, stronger twinning is observed, as expected, in samples of higher molecular weight.

Figs. 13 and 14 present the evolution of lamellar orientation of samples of H-2 and L-3, deformed to various strain at $T=80$ °C. Comparing these patterns with patterns

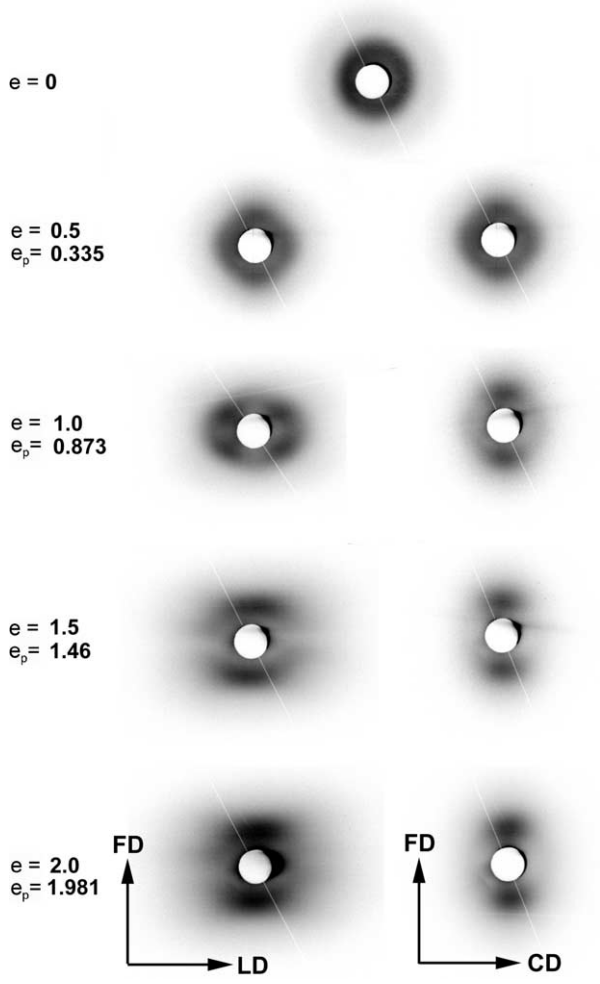

Fig. 13. Evolution of the SAXS patterns as a function of the strain, determined for linear homopolymer H-2, deformed at temperature of 80 °C. Left-side column-CD view, right-side column-LD view. Applied strain, e, and permanent strain, e_p, are indicated for each specimen.

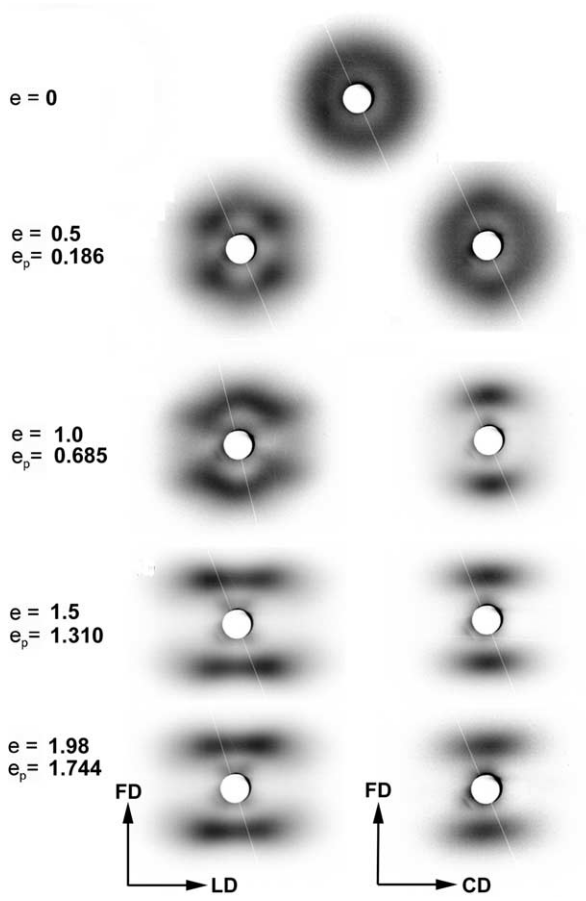

Fig. 14. Evolution of the SAXS patterns as a function of the strain, determined for branched homopolymer L-3, deformed at temperature of 80 °C. Left-side column-CD view, right-side column-LD view. Applied strain, e, and permanent strain, e_p, are indicated for each specimen.

shown in Figs. 6 and 7 (deformation at room temperature) one can see again that the respective patterns demonstrate similar features at respective strains. This indicates independence of the evolution of lamellar structure and its orientation on the temperature of deformation. These seem to depend solely on the strain applied, similarly to texture of crystals. One can conclude that the same deformation mechanisms have to operate at a given strain, independently on temperature of the process and related stress level.

5. Conclusions

The SAXS and WAXS studies of a series of various polyethylenes and ethylene-based copolymers, covering a broad range of chain architecture, molecular weight and crystallinity show their very similar orientation behavior. It can be concluded that the same deformation micro-mechanisms are involved in the deformation process of nearly all polymers studied. The only one exception found was elastomeric E-2 copolymer, which crystallizes in monoclinic modification rather than in common

orthorhombic form, and exhibits very low crystallinity, below 10% by volume.

The experimental results evidenced that the main deformation mechanisms of samples consisting of orthorhombic crystals are the (100)[001] and (100)[010] crystallographic slips supported by the deformation of amorphous component by interlamellar sliding. These mechanism lead to the formation of the primary texture component with chain axis aligned well along flow direction, FD, and (100) planes perpendicular to LD. However, a second texture component arises on unloading by {310} twinning of primary (100)[001] component. This second component is due to tensile stress along LD, generated during strain recovery on unloading. Intensity of twinning, hence the fraction of the twin component in the final texture depends on the stress generated during final stage of deformation (strain hardening), which determines the stress level during the strain recovery process. This strain hardening, resulting primarily from orientation of molecular network within amorphous component, is controlled in turn by the molecular weight of polymer and secondly by the degree of chain branching, both influencing properties of the molecular network. For samples of comparable crystallinity the fraction of twinned crystals increases with an increasing molecular weight. Molecular weight influences also the orientation behavior on the lamellar level. In all polymers studied the interlamellar shear is intense on the beginning of deformation and then exhausts and 'locks' around the true strain of 0.75. This brings to a limited fragmentation of lamellae by cooperative kinks, which helps to relieve some of constraints and allows further shear deformation. Further advance of that shear soon leads to another 'lock' of amorphous component which in polymers of relative low molecular weight results in much more massive fragmentation of the lamellae, thinned due to advanced crystallographic slips, and restructurization (by rotation of blocks) into new long period in the direction of flow, all at the strain around 1.2. In polymers of higher molecular weight such an intense fragmentation does not occur due to more constrained topological structure, consisting of large fraction of tie molecules and chain segments trapped between numerous entanglements, leading to high connectivity among neighboring lamellae. Consequently, the final structure of heavily deformed polyethylenes of low molecular weight consist of relatively small blocks, oriented with their normals approximately along FD, frequently outlined in a chevron-like pattern, which is a remnant of previous stage produced by deformation of kinked lamellae. Polyethylenes of higher molecular weight, in absence of intense lamellae fragmentation, develop the structure of relatively long, kinked lamellar crystals, arranged in a chevron-like structure.

It was found that the orientation produced by deformation process is controlled primarily by the strain applied to the material, while the differences produced by the modification of the stress due to the change of deformation temperature, or alternatively deformation rate, are of minor consequence.

Acknowledgements

Grant 7 T08E 036 19 from the State Agency for Scientific Research of Poland is acknowledged for partial financial support of this work.

References

[1] Bowden PB, Young R. J Mater Sci 1994;29:294–323.
[2] Lin L, Argon AS. J Mater Sci 1974;9:2034–51.
[3] Oleinik EF. Polym Sci, Ser C 2003;45:17–117.
[4] Pope DH, Keller A. J Polym Sci, Part B: Polym Phys 1975;13:533–66.
[5] Burnay GS, Groves GW. J Mater Sci 1978;13:639–46.
[6] Bartczak Z, Argon AS, Cohen RE. Macromolecules 1992;25:5036–53.
[7] Galeski A, Bartczak Z, Argon AS, Cohen RE. Macromolecules 1992;25:5705–18.
[8] Bartczak Z, Cohen RE, Argon AS. Macromolecules 1992;25:4692–704.
[9] Capaccio G, Ward IM. Polymer 1975;16:239–43.
[10] Capaccio G, Ward IM. Polymer 1974;15:233–8.
[11] Capaccio G, Crompton TA, Ward IM. J Polym Sci, Part B: Polym Phys Ed 1976;14:1641–58.
[12] Graham JT, Alamo RG, Mandelkern L. J Polym Sci, Part B: Polym Phys Ed 1997;35:213–23.
[13] Popli R, Mandelkern L. J Polym Sci, Part B: Polym Phys Ed 1987;25:441–83.
[14] Peacock AJ, Mandelkern L. J Polym Sci, Part B: Polym Phys Ed 1987;28:1917–41.
[15] Crist B, Fisher CJ, Howard PR. Macromolecules 1989;22:1709–18.
[16] Bensason S, Stepanov EV, Chum S, Hiltner A, Baer E. Macromolecules 1997;30:2436–44.
[17] Nitta K-h, Tanaka A. Polymer 2001;42:1219–26.
[18] Brooks NWJ, Mukhtar M. Polymer 2000;41:1475–80.
[19] Z.Bartczak., Polymer-submitted.
[20] Krause SJ, Hosford WF. J Polym Sci, Part B: Polym Phys Ed 1989;27:1853–65.
[21] Butler MF, Donald AM, Ryan AJ. Polymer 1998;39:781–92.
[22] Young RJ, Bowden PB, Ritchie JM, Rider JG. J Mater Sci 1973;8:23–36.
[23] Hoffman JD. Polymer 1983;24:3–26.
[24] Hoffman JD. Polymer 1982;23:656–70.
[25] Wunderlich B, Czornyj G. Macromolecules 1977;10:906–13.
[26] Hoffman JD, Miller RL. Polymer 1997;38:3151–212.
[27] Alexander LE. X-ray diffraction methods in polymer science. New York: Wiley-Interscience; 1969.
[28] Song HH, Argon AS, Cohen RE. Macromolecules 1990;23:870–6.
[29] Bartczak Z. J Appl Polym Sci 2002;86:1396–404.
[30] Boontongkong Y, Cohen RE, Spector M, Bellare A. Polymer 1998;39:6391–400.
[31] Seto T, Hara T, Tanaka K. Japan. J Appl Phys 1968;7:31–7.
[32] Russel KE, Hunter BK, Heyding RD. Polymer 1997;38:1409–14.
[33] Lewis D, Wheeler EJ, Maddams WF, Preedy JJ. J Polym Sci, Part A-2: Polym Phys 1972;10:369–74.